

# Artificial Neural Network based Modelling for Variational Effect on Double Metal Double Gate Negative Capacitance FET

Yash Pathak, Laxman Prasad Goswami *Student Member, IEEE*, Banshi Dhar Malhotra, *Member, IEEE*, and Rishu Chaujar, *Senior Member, IEEE*

**Abstract**—In this work, we have implemented an accurate machine-learning approach for predicting various key analog and RF parameters of Negative Capacitance Field-Effect Transistors (NCFETs). Visual TCAD simulator and the Python high-level language were employed for the entire simulation process. However, the computational cost was found to be excessively high. The machine learning approach represents a novel method for predicting the effects of different sources on NCFETs while also reducing computational costs. The algorithm of an artificial neural network can effectively predict multi-input to single-output relationships and enhance existing techniques. The analog parameters of Double Metal Double Gate Negative Capacitance FETs (D2GNCFETs) are demonstrated across various temperatures ( $T$ ), oxide thicknesses ( $T_{ox}$ ), substrate thicknesses ( $T_{sub}$ ), and ferroelectric thicknesses ( $T_{Fe}$ ). Notably, at  $T = 300K$ , the switching ratio is higher and the leakage current is 84 times lower compared to  $T = 500K$ . Similarly, at ferroelectric thicknesses  $T_{Fe} = 4nm$ , the switching ratio improves by 5.4 times compared to  $T_{Fe} = 8nm$ . Furthermore, at substrate thicknesses  $T_{sub} = 3nm$ , switching ratio increases by 81% from  $T_{sub} = 7nm$ . For oxide thicknesses at  $T_{ox} = 0.8nm$ , the ratio increases by 41% compared to  $T_{ox} = 0.4nm$ . The analysis reveals that  $T_{Fe} = 4nm$ ,  $T = 300K$ ,  $T_{ox} = 0.8nm$ , and  $T_{sub} = 3nm$  represent the optimal settings for D2GNCFETs, resulting in significantly improved performance. These findings can inform various applications in nanoelectronic devices and integrated circuit (IC) design.

**Index Terms**—Artificial Neural Network (ANN), NCFET, Machine learning, TCAD.

## I. INTRODUCTION

**S**INCE the 4 decades in the semiconductor industry, the size of FET devices has been decreased to attain better efficiency and performance, in possession with

This work was funded in part by the Council of Scientific and Industrial Research under Grant 08/133(0050)/2020-EMR-I for Yash, and BDM thanks the Science & Engineering Research Board (SERB), Govt. of India for the honor of a Renowned Fellowship (SB/DF/011/2019).

Y. Pathak and R. Chaujar are with the Department of Applied Physics, Delhi Technological University, Delhi, 110042 India (e-mail: yash\_2k19phdap505@dtu.ac.in; chaujar.rishu@dtu.ac.in).

L. P. Goswami is with the Department of Physics, Indian Institute of Technology, Delhi, 110016 India (e-mail: goswami.laxman@gmail.com).

B. D. Malhotra is with the Department of Biotechnology, Delhi Technological University, Delhi, 110042 India (e-mail: bansi.malhotra@dce.ac.in).

Moore's law [1]–[5]. The new trend of VLSI is governing the variability issue, such as global variability (GV) and local variability (LV) sources for both planar and gate-all-around (GAA) devices. In the case of LV source, a high- $k$ /metal gate device with various work functions, which is vital for statistical variability, would be at extreme risk for device performance because of the random occupied grain orientation of gate material [6], [7]. Additionally, in the case of the GV source, the impact of critical dimension is variability in varying the device performance, and as device size is reduced, this effect cannot be ignored.

The power and thermal management of integrated circuits (ICs) are vital aspects of the transistor industry. Although with engineering technology and material science advancement transistor generates a low amount of heat. However, the ICs have millions of transistors on the chip, which generate huge amounts of heat. Due to its lesser supply voltage, tunnel FETs have also been cited by many research organizations in the semiconductor world as the ideal FET over traditional MOSFETs for future low-power applications. But dealing with TFET can lead to low Ion, so to get the amalgamation of improved Ion and subthreshold swing, the NC technology is an apt candidate to meet the demand of future electronics. [4], [8]–[10].

However, the variability focuses on the accurate prediction of correlation among different sources. Cogenda Visual TCAD and Python are proven tools for doing complicated analysis [3,4]. However, a large number of samples is required for better performance. Hence, a large computational budget is inevitable for precise prediction. In this study, a method of variability analysis is proposed for modeling for device level as well as circuit level with minimum error [11]–[15]. Consequently, we propose a new method of machine learning (ML) algorithm with a precise match of the TCAD simulator for improved efficiency. This article consists of an analysis of analog parameters of D2GNCFET for different oxide thicknesses, ferroelectric thickness, temperature, and substrate thickness, which results in reduced subthreshold swing, low input power consumption, reduced leakage current, reduced drain-induced barrier lowering, and better controllability of the device.

## II. DEVICE ARCHITECTURE AND METHODOLOGY

Fig.1 shows the schematic diagram of the Double metal double gate NCFET (D2GNCFET) [16], [17]. The param-

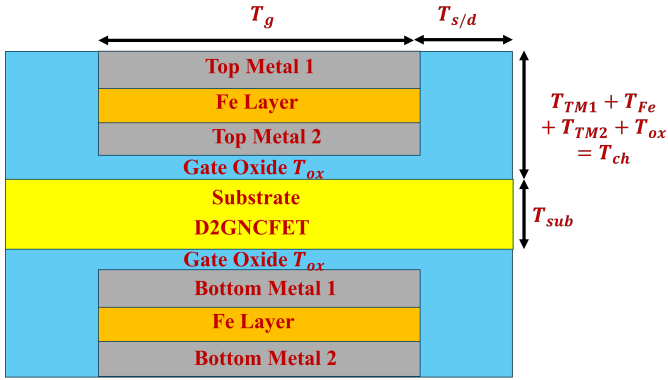


Fig. 1. The 2D schematic figure of double metal double gate NCFET.

TABLE I

THE DEVICE PARAMETERS FOR D2GNCFET ARE USED FOR THE SIMULATION

Parameter	Symbol	D2GNCFET
Substrate thickness	$T_{sub}$	5nm
Ferroelectric thickness	$T_{fe}$	7nm
Oxide Thickness	$T_{ox}$	0.6nm
Gate length	$L_g$	50nm
Concentration of Source/Drain	$N_{s/d}$	$10^{20} cm^{-3}$
Source/Drain length	$L_{s/d}$	5nm
Top/Bottom Metal thickness	$T_{m1}/T_{m1b}$	10nm

eters of D2GNCFET are summarized in table-I. The channel is made with silicon material and has a length of  $L_g = 60nm$ . The drain and source are made with aluminum which has length  $L_{d/s} = 50nm$ . The thickness of the substrate ( $T_{sub}$ ), oxide ( $T_{ox}$ ), top metal1/bottom metal1 ( $T_{TM1}/T_{TB1}$ ), top metal2/bottom metal2 ( $T_{TM2}/T_{TB2}$ ) are 5nm, 0.6nm, 10nm, 5nm respectively. The total thickness of channel ( $T_{ch}$ ) is 10nm as illustrated in table-I. The material of top metal1/bottom metal1, top metal2/bottom metal2 is Aluminium. The material taken for ferroelectric material, and gate oxide are  $HfO_2FE$ ,  $SiO_2$ . The work function ( $\phi$ ) of aluminum material is fixed at 4.2eV for the double gate. The concentration of the doping profile for Source/Drain ( $N_{s/d}$ ) is  $1.0 \times 10^{20} cm^{-3}$ .

The entire simulation is done by Cogenda Visual TCAD and Python high-level language. The gate voltage ( $V_{gs}$ ) is varied from 0 – 0.5V, with drain voltage fixed at 0.05V. The various physical models are used in this work, such as Shockley Read Hall (SRH) which includes generation and recombination effects, the Arora model which incorporates the effects on carrier mobility due to temperature and impurities concentration, Crowell size for consideration shows the impact ionization, Fermi Dirac statistics is used for improved efficiency and accuracy.

### III. ARTIFICIAL NEURAL NETWORK (ANN) IMPLEMENTATION

We constructed a tensor flow-based ANN model with a Rectified Linear Unit (ReLU) activation function [18]–[20] for D2GNCFET. The architecture of the ANN model is shown in Fig.2. The input to the input layer is an

array of size 5 for each variable Temperature  $T$ , Substrate thickness  $T_{sub}$ , Oxide thickness  $T_{ox}$ , Ferroelectric thickness  $T_{fe}$ , and the voltage  $V_{ds}$ . The output layer provides the ANN prediction for the drain current  $I_d$ . Further, we consider three hidden layers in our ANN model. The first and third layers have 256 neurons while there are 512 neurons in the middle layer. The output of each neuron in the Neural Network (NN) is given as:

$$a_p^{[q]} = g \left( \vec{W}_p^{[q]} \cdot \vec{a}^{[q-1]} + b_p^{[q]} \right) \quad (1)$$

where,  $q$  represents the layers of the neural network (NN), and  $p$  is the node number such that  $a_p^{[q]}$  is the output of  $p^{th}$  node from  $q^{th}$  layer.  $g$  is the activation function.  $\vec{W}$  and  $b$  are the weight and biasing parameters for each node.

This function is repeated and runs up to the Taylor series to get the precise result. The input value put in ANN does not exclude work function variation (WFV) due to WFV impact and varies the  $T_{ox}$ ,  $T$ ,  $T_{sub}$ ,  $T_{Fe}$  variability. In addition, it contains fixed parameters to study various dimensions of D2GNCFET. The algorithm of the implemented D2GNCFET ANN is illustrated in fig. 3.

### IV. RESULT AND DISCUSSION

Fig.4 represents the drain current ( $I_d$ ) vs gate voltage ( $V_{gs}$ ) of the TCAD simulation study (in red dash line) and predicted data (blue dash line) by ANN model for D2GNCFET at  $V_{ds} = 0.05V$ . The variation with oxide thickness ( $T_{ox}$ ) are displayed in subplots (a1)-(a4) at  $T_{Fe} = 7nm$ ,  $T = 300K$ ,  $T_{sub} = 5nm$ . The predicted and simulated data shows a precise match at  $T_{ox} = 0.6nm$ , which reflects the lower error at 0.3V of gate voltage. The variation with ferroelectric thickness ( $T_{Fe}$ ) is shown in subplots (b1)-(b4) at  $T_{ox} = 0.6nm$ ,  $T = 300K$ ,  $T_{sub} = 5nm$ . The precise data of predicted and simulated is matched at  $T_{Fe} = 8nm$ , reflecting the lower error after 0.3V of gate voltage. The variation with substrate thickness ( $T_{sub}$ ) is illustrated in subplots (c1)-(c4) at  $T_{ox} = 0.6nm$ ,  $T = 300K$ ,  $T_{Fe} = 7nm$ . The precise data of predicted and simulated is matched at  $T_{sub} = 4nm$ , which reflects the lower error at 0.3V of gate voltage. The variations with temperature is shown in subplots (d1)-(d4) at  $T_{ox} = 0.6nm$ ,  $T_{Fe} = 7nm$ , and  $T_{sub} = 5nm$ . The predicted and simulated data are matched at  $T = 300k$ , which reflects the minimum error after 0.3V of gate voltage. The different variations of all data variables turned out to coincide at gate voltage at 0.3V. The trainer of predicted data works successfully as a transfer characteristics start from off current to linear current.

Fig.5 shows the curve of output characteristics of D2GNCFET in linear and log scales for various temperatures and thicknesses. The device characteristics with variation in oxide thickness ( $T_{ox}$ ) are shown in Fig.5(a) at fixed  $V_{ds} = 0.05V$ ,  $T = 300K$ ,  $T_{Fe} = 7nm$ ,  $T_{sub} = 5nm$ . The better performance of the device is represented at  $T_{ox} = 0.8nm$ , which has a lower leakage current,

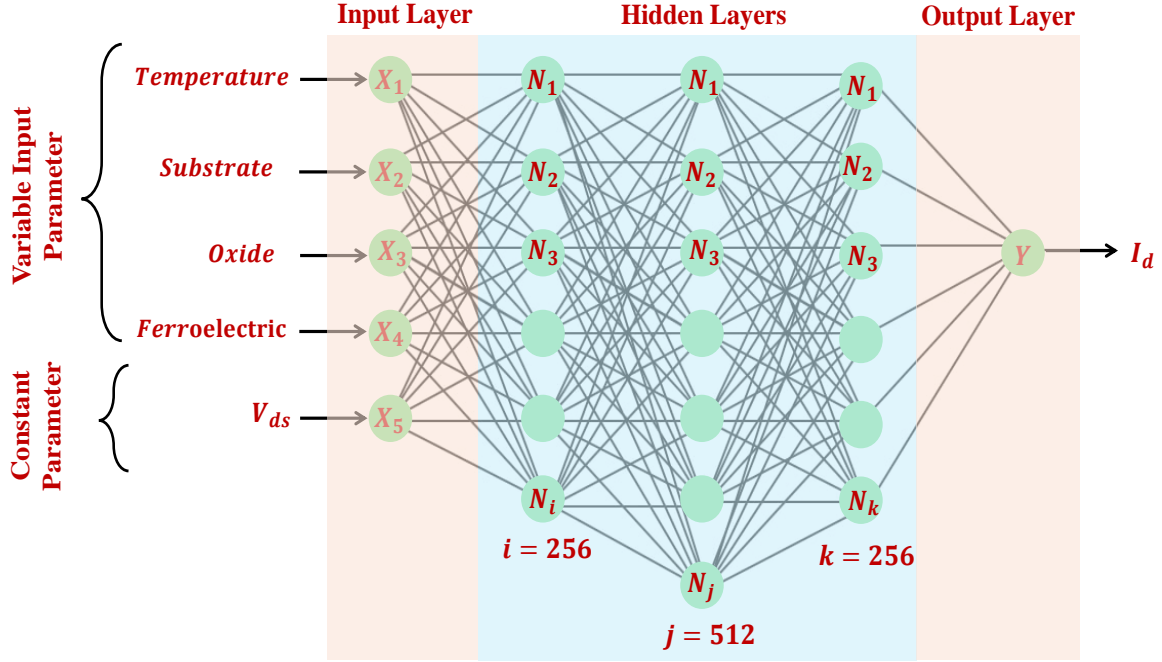


Fig. 2. The figure shows the D2GNCFET Artificial Neural Network (ANN) with one input, one output, and three hidden layers. There are 256 neurons in the first and third hidden layers, and 512 neurons in the middle layer. All I/O values include the source and the device parameter. The model predicts the drain current based on the input parameters Temperature, Substrate thickness, Oxide thickness, Ferroelectric thickness, and the drain-source voltage  $V_{ds}$ .

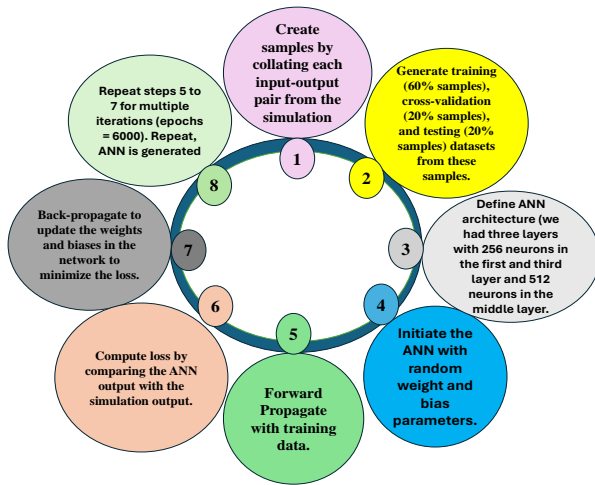


Fig. 3. Algorithm for D2GNCFET Artificial Neural Network (ANN)

higher drain current, and better switching ratio, confirming the improved gate controllability. The drain current of D2GNCFET is improved with higher oxide thickness. The impact of variation of ferroelectric thickness ( $T_{Fe}$ ) is shown in Fig.5(b) at fixed  $V_{ds} = 0.05V$ ,  $T = 300K$ ,  $T_{ox} = 0.6nm$ ,  $T_{sub} = 5nm$ . The better performance of the device is represented at  $T_{Fe} = 4nm$  with lower leakage current and higher drain current, resulting in a better switching

ratio with low power consumption. The drain current of D2GNCFET is improved with lesser ferroelectric thickness. The effect of variation of substrate thickness ( $T_{sub}$ ) is shown in Fig.5(c) at fixed  $V_{ds} = 0.05V$ ,  $T = 300K$ ,  $T_{ox} = 0.6nm$ ,  $T_{Fe} = 7nm$ . The better performance of the device is exhibited at  $T_{sub} = 3nm$ , which has a higher drain current, better switching ratio due to lower leakage current, and improved gate controllability. The drain current of D2GNCFET is improved with lesser substrate thickness. The influence of variation in temperature ( $T$ ) is shown in Fig.5(d) at fixed  $V_{ds} = 0.05V$ ,  $T_{Fe} = 7nm$ ,  $T_{ox} = 0.6nm$ , and  $T_{sub} = 5nm$ . The better performance of the device is represented at  $T = 300K$ , which has a lower leakage current and a higher drain current, thus ensuring a better switching ratio, improved gate controllability, and low power consumption. The drain current of D2GNCFET is improved at low temperatures.

The simulation and ANN prediction results are compared in Fig.6. The linear relation between the prediction and the TCAD simulation results signifies the accuracy of our ANN model as depicted in subplot Fig.6(a). We further computed the losses during each epoch of training the ANN model. The loss reduces by increasing the number of epochs as shown in subplot Fig.6(b).

Fig.7 shows the plot of transconductance and TGF as a function of gate voltage for various temperatures, and different thicknesses at  $V_{ds} = 0.05V$ ,  $T_{Fe} = 7nm$ ,

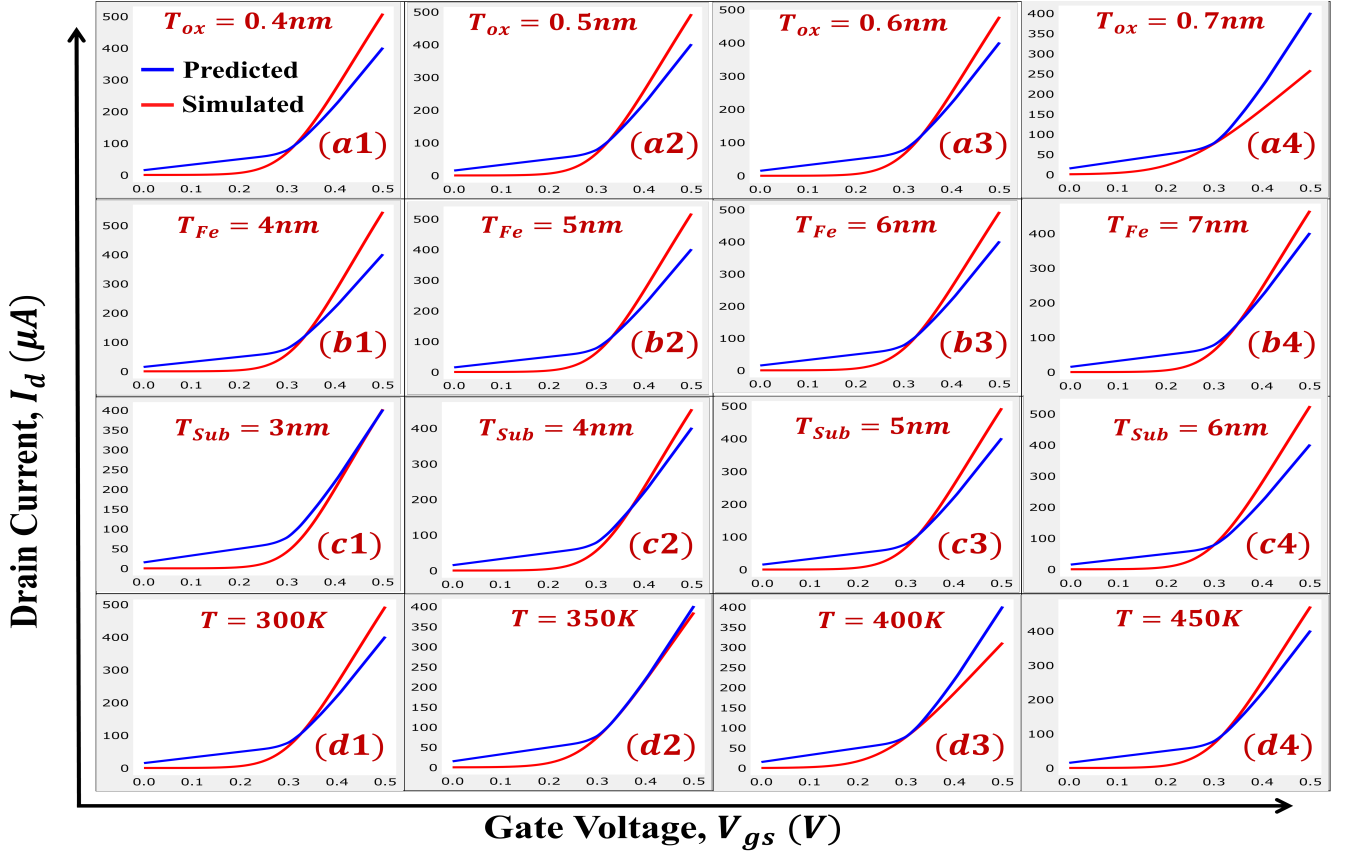


Fig. 4. The graph of drain current vs gate voltage for predicted and simulated data of D2GNCFET for different variations of temperature, oxide, thickness, ferroelectric thickness, substrate thickness at  $V_d=0.05V$ .

TABLE II  
D2GNCFET COMPARISON FOR TEMPERATURE, SUBSTRATE THICKNESS, FERROELECTRIC, OXIDE THICKNESS.

No.	Parameter	$I_{off}(10^{-8}A)$	$I_{on}/I_{off}(10^5)$	$V_{th}(mV)$	$SS(mV/dec.)$
(a1)	$T = 300k, T_{ox} = 0.4nm, T_{sub} = 5nm, T_{Fe} = 7nm$	1.92	0.273	77.23	76.121
(a2)	$T = 300k, T_{ox} = 0.5nm, T_{sub} = 5nm, T_{Fe} = 7nm$	1.62	0.314	82.278	75.464
(a3)	$T = 300k, T_{ox} = 0.7nm, T_{sub} = 5nm, T_{Fe} = 7nm$	1.25	0.383	89.52	74.33
(a4)	$T = 300k, T_{ox} = 0.8nm, T_{sub} = 5nm, T_{Fe} = 7nm$	1.13	0.412	92.18	73.86
(b1)	$T = 300k, T_{ox} = 0.6nm, T_{sub} = 5nm, T_{Fe} = 4nm$	0.382	1.52	118.2	68.4
(b2)	$T = 300k, T_{ox} = 0.6nm, T_{sub} = 5nm, T_{Fe} = 5nm$	0.605	0.89	107.77	70.53
(b3)	$T = 300k, T_{ox} = 0.6nm, T_{sub} = 5nm, T_{Fe} = 6nm$	0.935	0.55	97.2	72.69
(b4)	$T = 300k, T_{ox} = 0.6nm, T_{sub} = 5nm, T_{Fe} = 8nm$	2.08	0.227	76.065	77.061
(c1)	$T = 300k, T_{ox} = 0.5nm, T_{sub} = 3nm, T_{Fe} = 7nm$	0.523	0.768	115.107	72.22
(c2)	$T = 300k, T_{ox} = 0.5nm, T_{sub} = 4nm, T_{Fe} = 7nm$	0.906	0.5	99.462	73.719
(c3)	$T = 300k, T_{ox} = 0.5nm, T_{sub} = 6nm, T_{Fe} = 7nm$	2.06	0.2548	74.58	75.89
(c4)	$T = 300k, T_{ox} = 0.5nm, T_{sub} = 7nm, T_{Fe} = 7nm$	2.88	0.192	63.84	76.86
(d1)	$T = 300k, T_{sub} = 5nm, T_{Fe} = 7nm, T_{ox} = 0.5nm$	1.41	0.347	86.68	74.95
(d2)	$T = 350k, T_{sub} = 5nm, T_{Fe} = 7nm, T_{ox} = 0.5nm$	6.96	0.0553	40.23	87.55
(d3)	$T = 400k, T_{sub} = 5nm, T_{Fe} = 7nm, T_{ox} = 0.5nm$	0.225	0.0138	-5.21	100.498
(d4)	$T = 450k, T_{sub} = 5nm, T_{Fe} = 7nm, T_{ox} = 0.5nm$	0.55	0.0047	-50.04	113.927
(d5)	$T = 500k, T_{sub} = 5nm, T_{Fe} = 7nm, T_{ox} = 0.5nm$	0.011	0.0012	-94.86	128.28

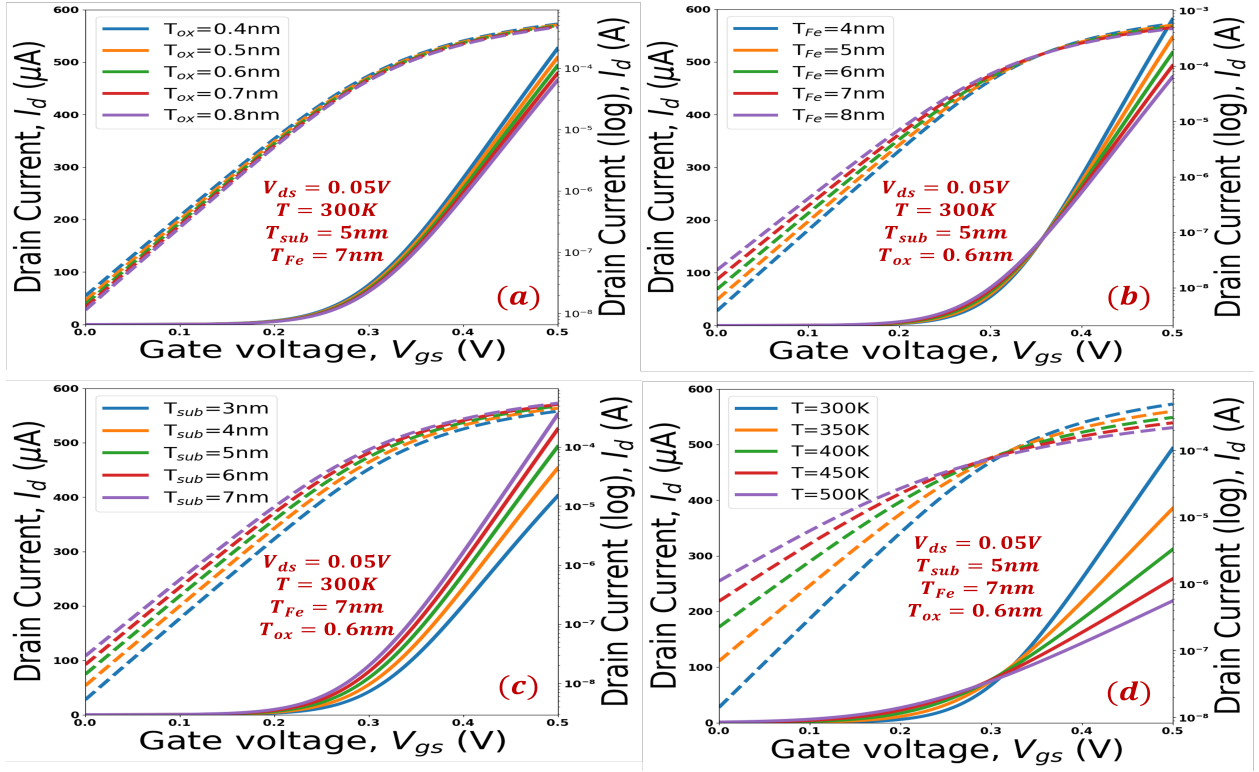


Fig. 5. The graph of drain current vs gate voltage D2GNCFET for different variations of temperature, oxide, thickness, ferroelectric thickness, substrate thickness at  $V_{ds}=0.05V$ .

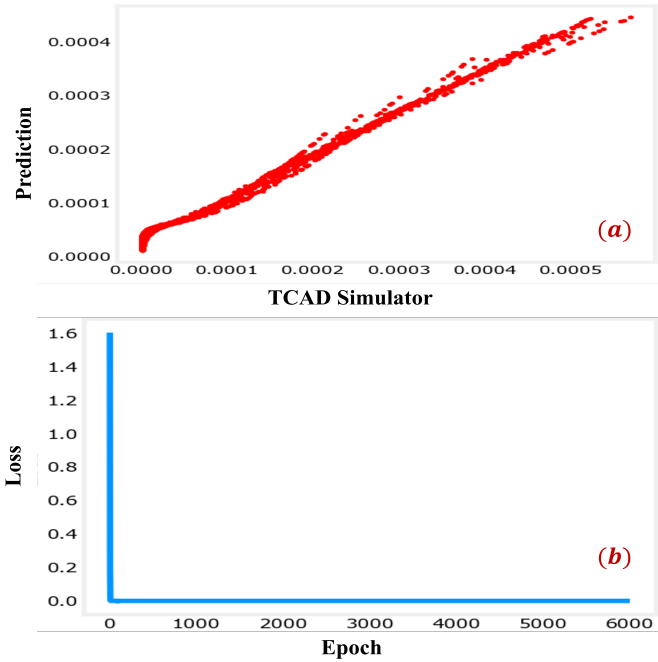


Fig. 6. The figure shows the comparison of TCAD simulated output and the output predicted by our ANN model. (a) The graph of predicted versus simulated data and (b) model loss at each epoch during the training of ANN model.

$T_{ox} = 0.6nm$ ,  $T = 300K$ ,  $T_{sub} = 5nm$ . The subplots (a) show the transconductance ( $g_m$ ) and transconductance gain factor (TGF) of D2GNCFET at  $T_{ox} = 0.8nm$  is higher than other oxide thickness, which reflects the high On current, better gain generated per unit cell, reduces the leakage current  $V_{ds} = 0.05V$ ,  $T_{Fe} = 7nm$ ,  $T = 300K$ ,  $T_{sub} = 5nm$ . The subplot (b) shows the transconductance ( $g_m$ ) and transconductance gain factor (TGF) of D2GNCFET at  $T_{Fe}=4nm$  is higher than other thickness of ferroelectric layer, which reveals the high On current, better gain generated per unit cell, reduces the leakage current  $V_{ds}=0.05V$ ,  $T=300K$ ,  $T_{ox}=0.6nm$ ,  $T_{sub}=5nm$ . The subplot (c) The transconductance ( $g_m$ ) and transconductance gain factor (TGF) of D2GNCFET at  $T_{sub}=3nm$  is higher than other thickness of substrate, which reflects the high On current, better gain generated per unit cell, reduces the leakage current  $V_{ds}=0.05V$ ,  $T_{Fe}=7nm$ ,  $T_{ox}=0.6nm$ ,  $T=300K$ . The subplot (d) The transconductance ( $g_m$ ) and transconductance gain factor (TGF) of D2GNCFET at  $T=300K$  is higher than the other temperatures, which reflects the high On current, better gain generated per unit cell, reduced the leakage current at  $V_{ds}=0.05V$ ,  $T_{Fe}=7nm$ ,  $T_{ox}=0.6nm$ ,  $T_{sub}=5nm$ .

Fig.8 spider chart of leakage current, on current, threshold voltage, SS for different temperatures, and thicknesses of different variable sets. (a) The oxide thickness of 0.8nm shows high On current, lower leakage current, higher threshold voltage, reduced subthreshold swing at  $V_{ds}=0.05V$ ,  $T_{Fe} = 7nm$ ,  $T_{sub} = 5nm$ ,  $T = 300K$ . (b)

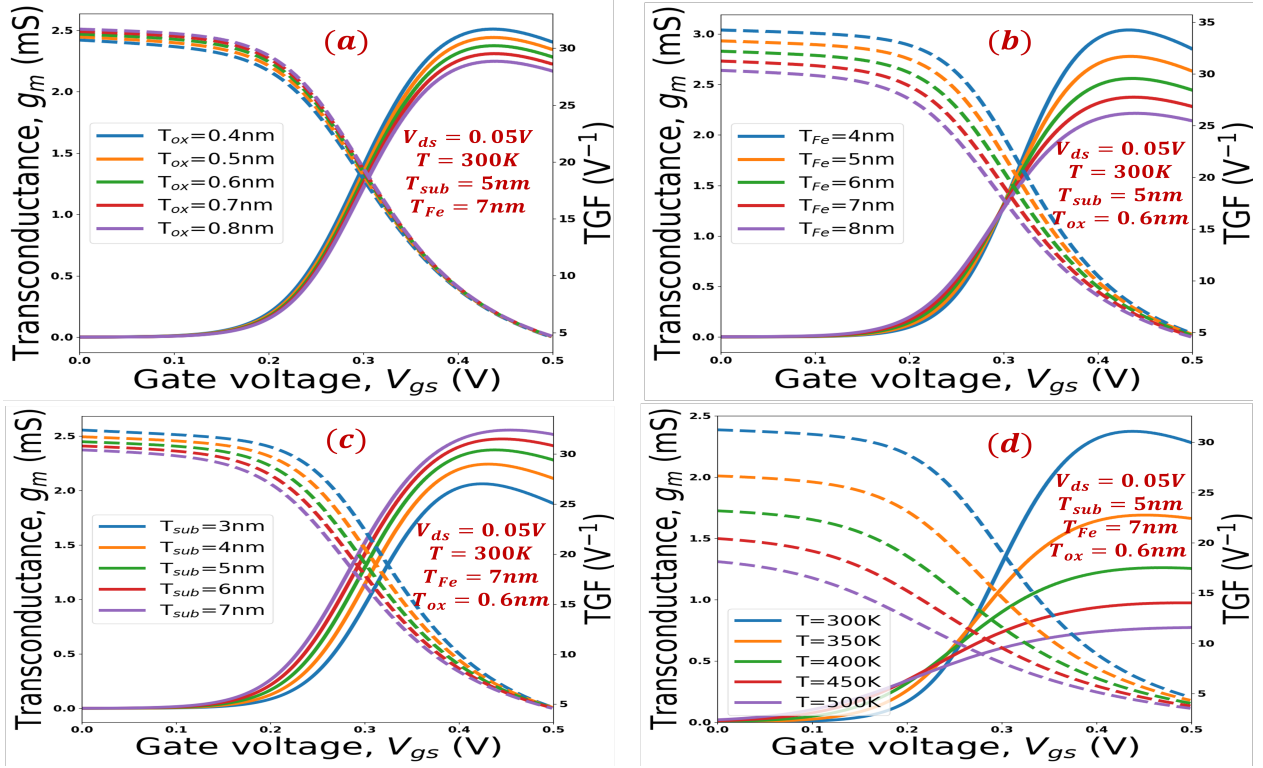


Fig. 7. The plot of transconductance and TGF vs  $V_{gs}$  for various temperature, thicknesses at  $V_d=0.05V$ .

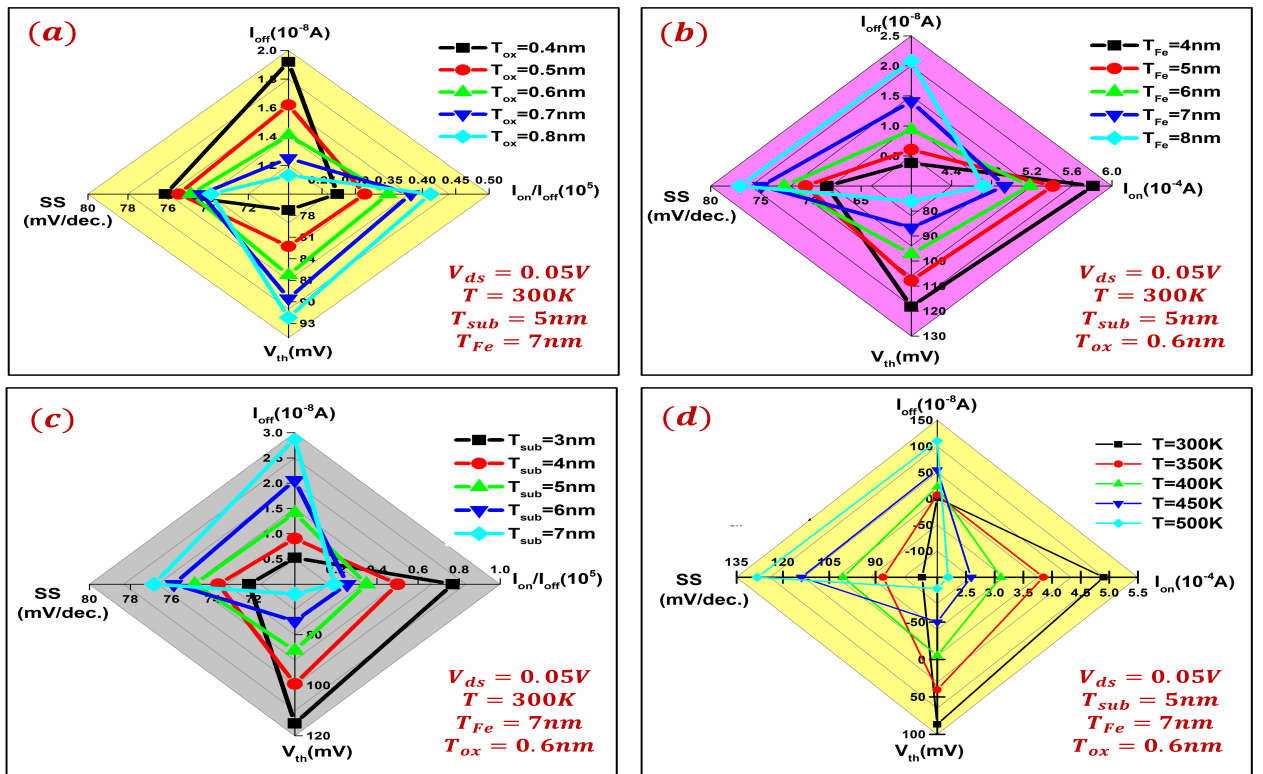


Fig. 8. The spider chart of leakage current, On current, Threshold Voltage, SS for different temperature, thicknesses at  $V_d=0.05V$ .

The ferroelectric thickness of  $4\text{nm}$  results in high On current, lower leakage current, higher threshold voltage, reduced subthreshold swing at  $V_{ds} = 0.05\text{V}$ ,  $T_{ox} = 0.6\text{nm}$ ,  $T_{sub} = 5\text{nm}$ ,  $T = 300\text{K}$ . (c) The substrate thickness of  $3\text{nm}$  showcases high On current, lower leakage current, higher threshold voltage, reduced subthreshold swing at  $V_{ds} = 0.05\text{V}$ ,  $T_{Fe} = 7\text{nm}$ ,  $T_{ox} = 0.6\text{nm}$ ,  $T = 300\text{K}$ . (d) The temperature of  $300\text{K}$  reflects high On current, lower leakage current, higher threshold voltage, reduced subthreshold swing at  $V_{ds} = 0.05\text{V}$ ,  $T_{Fe} = 7\text{nm}$ ,  $T_{sub} = 5\text{nm}$ ,  $T_{ox} = 0.6\text{nm}$ .

## V. CONCLUSION

In this study, we have analyzed ANN-based machine learning to access the freedom of variability in the ULSI domain. The Cogenda Visual TCAD simulator and Python high-level language are used throughout the process. The cost of computational work is substantially reduced by ANN-based ML with precise calculation and efficiency. The method investigating variability processes can help in better optimization and designing the useful for ULSI application. The analog parameter of D2GNCFET is studied for various oxide thickness, substrate thickness, temperature, and ferroelectric thickness, such as lower leakage current, higher switching ratio at  $T = 300\text{K}$  by 3000 times as compared to  $T = 500\text{K}$ , at  $T_{Fe} = 4\text{nm}$  by 588% in contrast at  $T_{Fe} = 8\text{nm}$ , at  $T_{sub} = 3\text{nm}$  by 300% in comparison at  $T_{sub} = 7\text{nm}$ ,  $T_{ox} = 0.8\text{nm}$  by 50% from  $T_{ox} = 0.4\text{nm}$ . All the analyzed results reveal that  $T_{Fe} = 4\text{nm}$ ,  $T = 300\text{K}$ ,  $T_{ox} = 0.8\text{nm}$ ,  $T_{sub} = 3\text{nm}$  as the most optimum set of variable sources for the D2GNCFET with the most improved performance and can further be used for various applications in nanoelectronic devices and IC designing.

## ACKNOWLEDGMENT

The authors thanks to Vinod Dham Centre of Excellence for Semiconductors and Microelectronics (VDCE4SM), Nano Bioelectronics and Microelectronics Lab, Delhi Technological University for giving essential facilities.

## REFERENCES

- [1] K. Ko, J. K. Lee, M. Kang, J. Jeon, and H. Shin, "Prediction of process variation effect for ultrascaled gaa vertical fet devices using a machine learning approach," *IEEE Transactions on Electron Devices*, vol. 66, no. 10, pp. 4474–4477, 2019.
- [2] X. Wang, B. Cheng, D. Reid, A. Pender, P. Asenov, C. Millar, and A. Asenov, "Finfet centric variability-aware compact model extraction and generation technology supporting dtco," *IEEE Transactions on Electron Devices*, vol. 62, no. 10, pp. 3139–3146, 2015.
- [3] X. Wang, B. Cheng, A. R. Brown, C. Millar, J. B. Kuang, S. Nassif, and A. Asenov, "Interplay between process-induced and statistical variability in 14-nm cmos technology double-gate soi finfets," *IEEE Transactions on Electron Devices*, vol. 60, no. 8, pp. 2485–2492, 2013.
- [4] S. B. Rahi, S. Tayal, and A. K. Upadhyay, "A review on emerging negative capacitance field effect transistor for low power electronics," *Microelectronics Journal*, vol. 116, p. 105242, 2021.
- [5] L. Gerrer, S. M. Amoroso, P. Asenov, J. Ding, B. Cheng, F. Adamu-Lema, S. Markov, A. Asenov, D. Reid, and C. Millar, "Interplay between statistical reliability and variability: A comprehensive transistor-to-circuit simulation technology," in *2013 IEEE International Reliability Physics Symposium (IRPS)*. IEEE, 2013, pp. 3A–2.
- [6] X. Wang, A. R. Brown, B. Cheng, and A. Asenov, "Statistical variability and reliability in nanoscale finfets," in *2011 International electron devices meeting*. IEEE, 2011, pp. 5–4.
- [7] H. F. Dadgour, K. Endo, V. K. De, and K. Banerjee, "Grain-orientation induced work function variation in nanoscale metal-gate transistors—part i: Modeling, analysis, and experimental validation," *IEEE Transactions on Electron Devices*, vol. 57, no. 10, pp. 2504–2514, 2010.
- [8] C.-I. Lin, A. I. Khan, S. Salahuddin, and C. Hu, "Effects of the variation of ferroelectric properties on negative capacitance fet characteristics," *IEEE transactions on electron devices*, vol. 63, no. 5, pp. 2197–2199, 2016.
- [9] Y. Pathak, B. D. Malhotra, and R. Chaujar, "Dft based atomic modeling and analog/rf analysis of ferroelectric hfo2 based improved fet device," *Physica Scripta*, vol. 98, no. 8, p. 085933, 2023.
- [10] K. Verma and R. Chaujar, "Analysis of vertically stacked ferroelectric based finfet for switching applications," in *2023 2nd International Conference on Futuristic Technologies (INCOFT)*. IEEE, 2023, pp. 1–4.
- [11] T. Hayasaka, A. Lin, V. C. Copa, L. P. Lopez Jr, R. A. Loberternos, L. I. M. Ballesteros, Y. Kubota, Y. Liu, A. A. Salvador, and L. Lin, "An electronic nose using a single graphene fet and machine learning for water, methanol, and ethanol," *Microsystems & nanoengineering*, vol. 6, no. 1, p. 50, 2020.
- [12] K. Ko, J. K. Lee, M. Kang, J. Jeon, and H. Shin, "Prediction of process variation effect for ultrascaled gaa vertical fet devices using a machine learning approach," *IEEE Transactions on Electron Devices*, vol. 66, no. 10, pp. 4474–4477, 2019.
- [13] T. Wu and J. Guo, "Multiobjective design of 2-d-material-based field-effect transistors with machine learning methods," *IEEE Transactions on Electron Devices*, vol. 68, no. 11, pp. 5476–5482, 2021.
- [14] Y. Pathak, P. Mishra, M. Sharma, S. Solanki, V. V. Agarwal, R. Chaujar, and B. D. Malhotra, "Experimental circuit design and tcad analysis of ion sensitive field effect transistor (isfet) for ph sensing," *Materials Science and Engineering: B*, vol. 299, p. 116951, 2024.
- [15] Y. Pathak, B. D. Malhotra, and R. Chaujar, "Detection of biomolecules in dielectric modulated double metal below ferroelectric layer fet with improved sensitivity," *Journal of Materials Science: Materials in Electronics*, vol. 33, no. 17, pp. 13558–13567, 2022.
- [16] G. Pahwa, T. Dutta, A. Agarwal, and Y. S. Chauhan, "Physical insights on negative capacitance transistors in nonhysteresis and hysteresis regimes: Mfmis versus mfis structures," *IEEE Transactions on Electron Devices*, vol. 65, no. 3, pp. 867–873, 2018.
- [17] G. Pahwa, A. Agarwal, and Y. S. Chauhan, "Numerical investigation of short-channel effects in negative capacitance mfis and mfmis transistors: Subthreshold behavior," *IEEE Transactions on Electron Devices*, vol. 65, no. 11, pp. 5130–5136, 2018.
- [18] K. Hara, D. Saito, and H. Shouno, "Analysis of function of rectified linear unit used in deep learning," in *2015 international joint conference on neural networks (IJCNN)*. IEEE, 2015, pp. 1–8.
- [19] S. Das, K. Saxena, J.-C. Tinguely, A. Pal, N. L. Wickramasinghe, A. Khezri, V. Dubey, A. Ahmad, V. Perumal, R. Ahmad, et al., "Sers nanowire chip and machine learning-enabled classification of wild-type and antibiotic-resistant bacteria at species and strain levels," *ACS Applied Materials & Interfaces*, vol. 15, no. 20, pp. 24047–24058, 2023.
- [20] T. Kessler, G. Dorian, and J. H. Mack, "Application of a rectified linear unit (relu) based artificial neural network to cetane number predictions," in *Internal Combustion Engine Division Fall Technical Conference*, vol. 58318. American Society of Mechanical Engineers, 2017, p. V001T02A006.